ORIGINAL ARTICLE

A new global grid model for the determination of atmospheric weighted mean temperature in GPS precipitable water vapor

Liangke Huang[1,2] · Weiping Jiang[1] · Lilong Liu[2,3] · Hua Chen[4] · Shirong Ye[1]

Abstract

In ground-based global positioning system (GPS) meteorology, atmospheric weighted mean temperature, T_m, plays a very important role in the progress of retrieving precipitable water vapor (PWV) from the zenith wet delay of the GPS. Generally, most of the existing T_m models only take either latitude or altitude into account in modeling. However, a great number of studies have shown that T_m is highly correlated with both latitude and altitude. In this study, a new global grid empirical T_m model, named as GGTm, was established by a sliding window algorithm using global gridded T_m data over an 8-year period from 2007 to 2014 provided by TU Vienna, where both latitude and altitude variations are considered in modeling. And the performance of GGTm was assessed by comparing with the Bevis formula and the GPT2w model, where the high-precision global gridded T_m data as provided by TU Vienna and the radiosonde data from 2015 are used as reference values. The results show the significant performance of the new GGTm model against other models when compared with gridded T_m data and radiosonde data, especially in the areas with great undulating terrain. Additionally, GGTm has the global mean RMS_{PWV} and RMS_{PWV}/PWV values of 0.26 mm and 1.28%, respectively. The GGTm model, fed only by the day of the year and the station coordinates, could provide a reliable and accurate T_m value, which shows the possible potential application in real-time GPS meteorology, especially for the application of low-latitude areas and western China.

Keywords GGTm model · GGOS · GPT2w model · Precipitable water vapor · GPS meteorology

Abbreviations

GGOS	Global geodetic observing system
GPS	Global positioning system
GNSS	Global navigation satellite system
GGTm	Global grid T_m model
GPT	Global pressure and temperature
GPT2w	Global pressure and temperature 2 wet
ECMWF	European Centre for Medium-Range Weather Forecasts
NCEP	National Centers for Environmental Prediction
PWV	Precipitable water vapor
ZTD	Zenith total delay
ZWD	Zenith wet delay
ZHD	Zenith hydrostatic delay
RMS	Root mean square
IGS	International GNSS Service

✉ Weiping Jiang
wpjiang@whu.edu.cn

[1] GNSS Research Center, Wuhan University, Wuhan 430079, China

[2] College of Geomatics and Geoinformation, Guilin University of Technology, Guilin 541004, China

[3] Guangxi Key Laboratory of Spatial Information and Geomatics, Guilin 541004, China

[4] School of Geodesy and Geomatics, Wuhan University, Wuhan 430079, China

1 Introduction

Water vapor, an important component of the Earth's atmosphere, plays a key role in global atmospheric radiation, water cycling and energy balance (Wang et al. 2007; Wang and Zhang 2009; Jin and Luo 2009). Understanding the spatial and temporal distribution of water vapor in the atmosphere is of great scientific and practical significance in weather forecasting and climate prediction. Traditional techniques for detecting water vapor mainly include water vapor radiometers, radiosondes and remote sensing. These methods are

unable to meet the increasing demands of modern meteorological development, primarily due to the expensive devices, heavy workload and low spatiotemporal resolution.

A global positioning system (GPS) technique has advantages of all-weather conditions, high precision and wide coverage and has been fully operational since 1994. The GPS signal path through the Earth's atmosphere is influenced by troposphere refraction, resulting in a GPS signal delay, i.e., a tropospheric delay. The tropospheric delay can be expressed as zenith total delay (ZTD) multiplied by the tropospheric mapping function. Meanwhile, the ZTD consists of two parts: zenith hydrostatic delay (ZHD) and zenith wet delay (ZWD). Precipitable water vapor (PWV) is the total precipitation of the vapor content in a unit area cylinder from the ground to the outer layer of the atmosphere (Chen et al. 2014). Bevis et al. (1992) first proposed the concept of GPS meteorology and developed an approach to calculate the crucial parameter, weighted mean temperature (T_m), for retrieving the PWV from the ZWD of GPS. The ZTD can be calculated precisely using GPS measurements, and the ZHD can also be determined using a tropospheric empirical model. Then, ZWD can be computed by subtracting ZHD from ZTD. Therefore, the GPS technique becomes a powerful method to detect atmospheric water vapor with advantages of high precision, real time and high spatiotemporal resolution. The relationship between ZWD and PWV can be expressed as follows (Askne and Nordius 1987; Bevis et al. 1994; Ross and Rosenfeld 1997):

$$PWV = \Pi \cdot ZWD \tag{1}$$

where Π is a conversion factor, with an expression as follows:

$$\Pi = \frac{10^6}{\rho_w R_v \left(\frac{k_3}{T_m} + k_2' \right)} \tag{2}$$

where R_v is the specific gas constant for water vapor; ρ_w is the density of water; k_2' and k_3 are the atmospheric refractivity constants given in Bevis et al. (1994); and T_m is the weighted mean temperature and the key variable to determine the conversion factor Π (Bevis et al. 1992). According to the law of error propagation, the precision of calculated PWV is mainly affected by the error sources of T_m and ZWD based on Eqs. (1) and (2). Equations (3) and (4) could provide an explanation of how the errors from T_m and ZWD affect PWV.

$$\sigma_{PWV} = \Pi \cdot \sigma_{ZWD} + ZWD \cdot \sigma_{\Pi} \tag{3}$$

$$\sigma_{\Pi} = \frac{10^6 k_3}{\rho_w R_v \left(k_3 + k_2' T_m \right)^2} \sigma_{T_m} \tag{4}$$

where σ_{PWV}, σ_{ZWD}, σ_{T_m} and σ_{Π} are errors from PWV, ZWD, T_m and Π, respectively. Currently, the precision of the ZTD product provided by the International GNSS Service (IGS) is better than 5 mm (Byun and Bar-Sever 2009). The ZHD can be accurately estimated using surface pressure measurements or numerical weather models (Hobiger et al. 2008a; Lu et al. 2016; Zhang et al. 2017), while for the application of real-time/near real-time mode, one can use a short-range forecast from a weather model (e.g., the forecast VMF1) to derive ZHD (Hobiger et al. 2008b; Lu et al. 2017). Thus, the ZWD can achieve a remarkable accuracy. If the ZWD has an error of 1 cm, the error of calculated PWV caused by ZWD error is approximately 1.5 mm (Yao et al. 2014a), and the accuracy of T_m is considered one of the largest error sources in PWV estimation. Bevis et al. (1994) indicated that the relative error of Π is basically equal to that of T_m. Precisely estimating T_m, therefore, is the key to improving the accuracy of PWV calculation.

Generally, in post-processing mode the T_m can be exactly determined using atmospheric profiles (such as water vapor pressure and temperature) based on integration, while in real-time/near real-time mode the T_m can also be derived using fairly accurate atmospheric profiles from numerical weather models (Lu et al. 2017). However, to enhance the efficiency of T_m calculation and provide convenience for users, an accurate T_m empirical model is needed to meet such demands. Bevis et al. (1992) conducted an analysis of the correlation between surface temperature (T_s) and T_m using 8718 radiosonde profiles in North America, and they found that T_m and T_s have a good linear correlation; thus, the Bevis formula, $T_m = a + bT_s$, is a commonly used model to estimate T_m. In the Bevis formula, the coefficients of a and b are largely season- and location-dependent and should be estimated using meteorological measurements from specific areas and seasons (Bevis et al. 1992; Ross and Rosenfeld 1997; Emardson et al. 1998; Emardson and Derks 2000; Wang et al. 2011). Some regional linear functions of T_m and T_s were established in China (Li et al. 1999; Wang et al. 2011), and the coefficients of these functions were re-estimated using local radiosonde profiles with higher precision than that of the Bevis formula for local use. Similarly, Yao et al. (2014a) analyzed the correlation of T_m and T_s around the globe and established a global latitude-related linear regression model based on the gridded T_m data as provided by TU Vienna (abbreviated as gridded T_m data) and the European center for medium-range weather forecasts (ECMWF) T_s data, and the new model can obtain excellent results around the globe. Yao et al. (2014b) studied the relation between T_m and T_s, water vapor pressure (e_s) and surface pressure (P_s) and then developed one/multi-parameter T_m models that consider seasonal and geographic variations. The two models show better performance around the globe. The regression models can achieve great results if in situ meteorological

measurements are available. Unfortunately, meteorological sensors are not installed at most GPS stations, and the linear regression models of T_m and T_s become invalid in real-time application of GPS meteorology because the in situ T_s measurements are unavailable.

In recent years, the PWV retrieved from GPS signal is widely used for the analysis or nowcasting of severe weather conditions such as heavy rainfall, flood, deep convective and typhoon events (Sapucci et al. 2016; Huelsing et al. 2017; Adams et al. 2013; Zhao et al. 2018), because of its high accuracy, high temporal resolution and all-weather conditions. An accurate real-time GPS-PWV estimation is helpful to improve weather for- and now casting. Thus, an empirical model is needed to provide a real-time T_m value for retrieving real-time GPS-PWV. Emardson and Derks (2000) developed an empirical T_m model in Europe that considers the latitude and annual variations of T_m, and it could be used largely in real-time GPS meteorology as it is without any meteorological parameters for input. Yao et al. (2015a) established an improved atmospheric conversion factor model in low-latitude China by considering the height variation in the model of Emardson and Derks (2000). Zhang et al. (2017) established two enhanced T_m models, GM-T_m (a mixed-grid model) and GH-T_m, using ERA-Interim data sets over China. These two models both show a high accuracy over China. To improve the global applicability of the model, extensive researches have been conducted for global T_m modeling. Yao et al. (2012) developed the Global Weighted Mean Temperature (GWMT) model based on radiosonde data of 135 global sites, but due to the uneven distribution of the global radiosonde sites (no radiosonde sites in oceanic areas), it cannot obtain sufficient accuracy in the southern Pacific Ocean. To overcome these problems, however, an improved model, GTm-II, was proposed by re-estimating the coefficients using T_m from the Bevis formula over oceanic areas (Yao et al. 2013), where T_s is calculated from the global pressure and temperature (GPT) model (Böhm et al. 2007). Chen et al. (2014) proposed an improved T_m model, GTm_N, using the America National Centers for Prediction (NCEP) reanalysis data, which takes the influence of annual and semi-annual periodicity of T_m into account. Similarly, Yao et al. (2015b) developed the GWMT-G model by improving the GTm-II using gridded T_m data. The GTm-II model was further improved (taking semi-annual and diurnal variations into account) into GTm-III (Yao et al. 2014c). Because the lapse rate of T_m, in most cases, is neglected in some empirical models, He et al. (2017) developed an empirical grid T_m model, GWMT-D, based on the annual, semi-annual and diurnal variations in T_m. Because it takes the lapse rate of T_m into account, the new model shows excellent performance at different altitudes all over the globe. In addition, the newly released empirical tropospheric delay models, such as the GPT2w model (Böhm et al. 2015) and ITG model (Yao et al. 2015c), also provide a precise T_m product.

The purpose of this study is to develop a global T_m empirical model for providing accurate real-time T_m value to derive an accurate real-time PWV estimate. As previously analyzed, T_m shows apparent season and location dependence over the globe, and also it presents a high correlation with both latitude and altitude. The model equations of the existing T_m models, as mentioned, only take one spatial factor into account, i.e., either latitude or altitude. In this study, both latitude and altitude variations are considered in modeling, and a new global grid T_m model, GGTm, will be developed based on the sliding window algorithm using gridded T_m data and global ellipsoidal height grid data.

2 Methods for calculating T_m

Two data sets are used to estimate T_m: gridded T_m data and radiosonde profiles. Gridded T_m data from 2007–2014 are used to establish the new GGTm model, while both gridded T_m data and radiosonde profiles in 2015 are used to evaluate the GGTm model as well as the Bevis formula and GPT2w model.

2.1 Computing T_m based on radiosonde profiles

The radiosonde technique is one of the most common methods to measure meteorological parameters. The radiosonde data mainly contain surface parameters (such as T_s, P_s and PWV) and pressure level parameters (such as geopotential height H, relative humidity RH and absolute temperature T at every pressure level) at UTC 00:00 and 12:00 every day. Currently, there are in total more than 1500 radiosonde sites distributed over the globe. The radiosonde profiles can be retrieved free from the upper-air archive at the websites of the University of Wyoming (http://weather.uwyo.edu/upperair/sounding.html) or the Integrated Global Radiosonde Archive (IGRA) (http://www.ncdc.noaa.gov/oa/climate/igra/). The T_m values are obtained through numerical integration using geopotential height, absolute temperature and relative humidity measurements at every pressure level along the zenith direction. The formula to calculate T_m can be expressed as follows:

$$T_m = \frac{\int (e/T)\, dH}{\int (e/T^2)\, dH} \tag{5}$$

where T is the absolute temperature (K) and e is the water vapor pressure (hPa), as radiosonde profiles provide the relative humidity RH and absolute temperature T (K), which

can be used to calculate the e (hPa) in the following formula (Bolton 1980; Wang et al. 2016):

$$e = \frac{\text{RH} \cdot e_s}{100} \tag{6}$$

$$e_s = 6.11 \times 10^{\left(\frac{7.5 \times T_d}{237.3 + T_d}\right)} \tag{7}$$

where e_s is the saturated vapor pressure and T_d is the atmospheric temperature in Celsius ($T = T_d + 273.15$). In practice, Eq. (5) will be discretized using the following integral formula:

$$T_m = \frac{\int (e/T) \, dH}{\int (e/T^2) \, dH} = \frac{\sum_1^n \psi(e_i, T_i) \, \Delta h_i}{\sum_1^n \phi(e_i, T_i) \, \Delta h_i} \tag{8}$$

where $\psi(e_i, T_i) = \frac{e_i}{T_i}$, $\phi(e_i, T_i) = \frac{e_i}{T_i^2}$; Δh_i indicates the thickness of the atmosphere at the ith layer (m), n is the number of layers; and T_i and e_i indicate the average temperature and water vapor pressure at the ith layer of the atmosphere, respectively.

2.2 Computing T_m based on the linear regression formula

Several researchers have noted that the relationship between T_m and T_s has a strong linear correlation over the globe (Bevis et al. 1992; Yao et al. 2014a); thus, T_m can be estimated using a linear function of T_s for a specific area. Bevis et al. (1994) developed the Bevis $T_m - T_s$ relationship using 2 years of radiosonde profiles from 13 radiosonde sites distributed in the United States, and the formula is as follows:

$$T_m = 70.2 + 0.72 T_s. \tag{9}$$

According to Eq. (9), T_m can easily be calculated from T_s, making it the most widely used T_m model. The relationship between T_m and T_s varies with season and location (Emardson and Derks 2000; Wang et al. 2005; Yao et al. 2014a), and the coefficients of the formula are estimated from radiosonde measurements in North America, while its accuracy would be affected when applied globally. Additionally, few GPS stations are equipped with meteorological sensors for measuring T_s, thus limiting its application in real-time GPS meteorology.

2.3 T_m derived from the GPT2w model

When modeling tropospheric delay or atmospheric weighted mean temperature, the resolution and accuracy of a model will be improved if the model parameters are stored in the form of a grid. Global pressure and temperature 2 wet (GPT2w), an empirical troposphere delay model, was developed by Böhm et al. (2015) using ERA-Interim data sets (the newest products of ECMWF). This empirical model, an improved model for GPT, can provide several tropospheric parameters, such as T_m, pressure, temperature and water vapor pressure with two horizontal resolutions of $1° \times 1°$ and $5° \times 5°$. T_m is calculated by the following equation:

$$\begin{aligned} T_m^{\text{GPT2W}} = {} & A_0 + A_1 \cos\left(\frac{\text{doy}}{365.25} 2\pi\right) \\ & + B_1 \sin\left(\frac{\text{doy}}{365.25} 2\pi\right) + A_2 \cos\left(\frac{\text{doy}}{365.25} 4\pi\right) \\ & + B_2 \sin\left(\frac{\text{doy}}{365.25} 4\pi\right) \end{aligned} \tag{10}$$

where doy is the day of year, and the other coefficients in this equation are determined based on a regular grid of $1° \times 1°$ and $5° \times 5°$. Thus far, GPT2w is one of the newest released models, which has excellent performance in the computation of tropospheric parameters against other models.

3 Construction of a new global grid T_m model: GGTm

Extensive studies, as mentioned in Sect. 1, have focused on establishing a regional T_m model using local radiosonde measurements, which undoubtedly can yield a better performance for local use but is not suitable globally. In recent years, several empirical global T_m models have been developed, and the parameters of these models are mainly expressed by spherical harmonics or are stored in the form of a grid. A fitting error of the model parameters will be introduced if using the spherical harmonics for global T_m modeling. For global grid models, i.e., models with the parameters stored in the form of a grid, the realization of the T_m calculation is usually accomplished by adopting bilinear interpolation after achieving four gridded coefficients around the site. These types of models generally have good results over the globe. As we know, a regional T_m model should be the recommended model in a specific area due to its superior performance, but how can one realize a regional T_m model for global application? Greater efforts were made here to derive a new approach.

3.1 Introduction of the sliding window algorithm

In this study, a new approach, the sliding window algorithm, will be introduced to solve the aforementioned problems or shortages. Yao et al. (2014a) conducted an analysis of the correlation between T_m and T_s over the globe using a sliding window algorithm. On a global scale, it can be divided into numerous regular areas (i.e., each area denotes one sliding
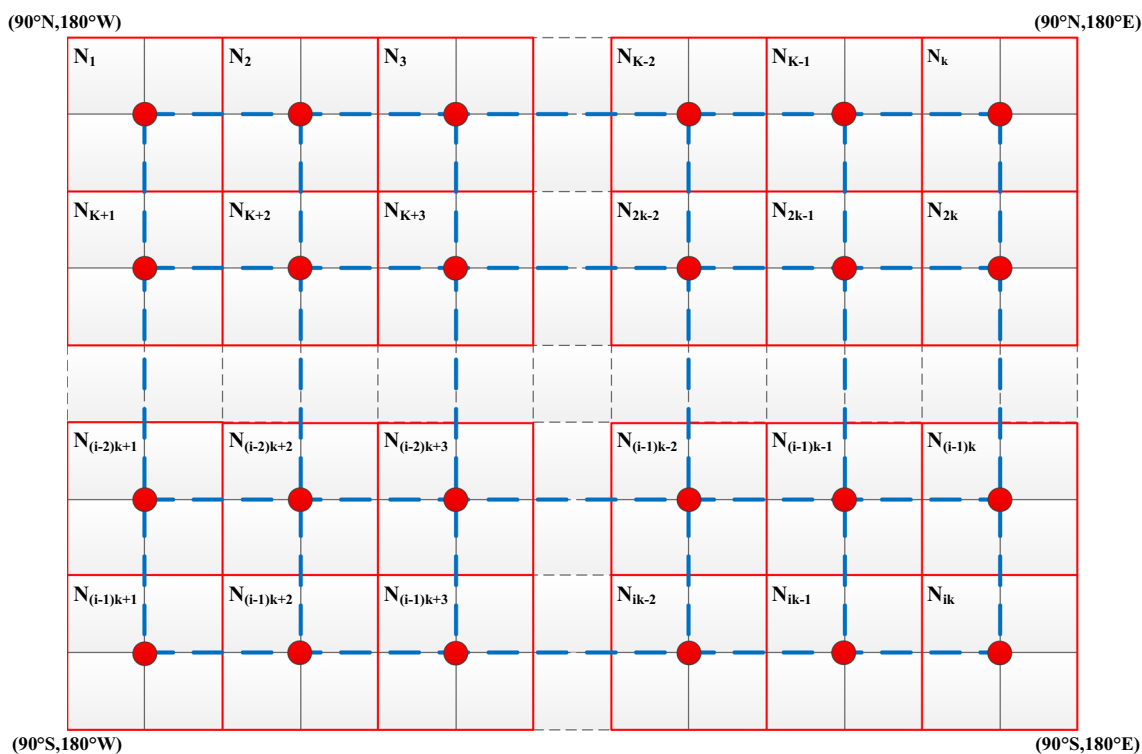
(90°N,180°W)   (90°N,180°E)

(90°S,180°W)   (90°S,180°E)

Fig. 1 The realization process of the sliding window algorithm over the globe (The figure is drawn using Microsoft Visio 2010)

window) of the same size by employing the sliding window algorithm.

In the sliding window algorithm, there are two key steps that need to be employed. The first step requires dividing the globe into a grid. In this work, the global gridded T_m data with a horizontal resolution of $2.5° \times 2°$ (lon. × lat.) are employed to compute the new model parameters. Hence, the globe can be divided into regular grids with the same quantities and horizontal resolution of gridded T_m data. The second step requires determining the size of the sliding window. The determination of window size is dependent on several factors, such as guaranteeing that the quantity of windows over the globe is an integer, maintaining continuity between windows and ensuring the computability of model parameters in each window. Considering these factors, we take the size of the sliding window as $5° \times 4°$ (lon. × lat.), as an example, to describe the realization process of the sliding window algorithm, as shown in Fig. 1. For each window, data at the 3×3 grid points in the sliding window are used to estimate model parameters, which will then be taken as results of the center point of the sliding window. First, calculate the model parameters of the sliding window N_1 at the upper-left corner as the results of the center point of window N_1 (the red rectangle denotes the size of the sliding window, and the red dot denotes the center point of each window, as shown in Fig. 1); then, moving the sliding window by two points along the latitude, calculate the model parameters of the sliding window

N_2 as the results of the center point of window N_2, continuing until the last sliding window N_k of this latitude. Moving the sliding window by two points along the longitude, and then calculate the model parameters of all sliding windows at this latitude according to the methods as previously mentioned, continuing until the model parameters of all sliding windows over the globe are calculated. Finally, a new global grid with a resolution of $5° \times 4°$ (lon. × lat.), which consists of red dots and blue dashed lines as shown in Fig. 1, will be created.

3.2 Expression of GGTm

There have been extensive studies conducted on the spatiotemporal characteristic of T_m, and the empirical T_m model was developed based on its characteristics. The characteristics of the time series of T_m mainly show annual and semi-annual variations (Wang et al. 2005; Chen et al. 2014; Böhm et al. 2015). While the diurnal variation in T_m is generally small, with mean amplitudes of 0.5–1.5 K over most land areas and less than 0.5 K over most oceans (Wang et al. 2005), it is also season- and location-dependent and is difficult to model precisely using simple trigonometric functions (He et al. 2017). For the spatial characteristic of T_m, the model equations of the existing T_m models, as mentioned in Sect. 1, only take one spatial factor into account (i.e., either latitude or altitude); in addition, T_m is slightly affected

by longitude (Yao et al. 2014b). As previously discussed, the GGTm considers annual and semi-annual variations and takes both latitude and altitude variations into account in the model expression of each window. The model expression of each window is as follows:

$$
\begin{aligned}
T_m\left(\varphi_U, \lambda_U, h, \mathrm{doy}\right) = {} & \alpha_1\left(\varphi_i, \lambda_i\right) \\
& + \alpha_2\left(\varphi_i, \lambda_i\right) \cdot \varphi_U + \alpha_3\left(\varphi_i, \lambda_i\right) \cdot h \\
& + \alpha_4\left(\varphi_i, \lambda_i\right) \cdot \cos\left(2\pi \frac{\mathrm{doy}}{365.25}\right) \\
& + \alpha_5\left(\varphi_i, \lambda_i\right) \cdot \sin\left(2\pi \frac{\mathrm{doy}}{365.25}\right) \\
& + \alpha_6\left(\varphi_i, \lambda_i\right) \cdot \cos\left(4\pi \frac{\mathrm{doy}}{365.25}\right) \\
& + \alpha_7\left(\varphi_i, \lambda_i\right) \cdot \sin\left(4\pi \frac{\mathrm{doy}}{365.25}\right)
\end{aligned}
\tag{11}
$$

where doy is the day of the year; (φ_i, λ_i) are the latitude (in degree) and longitude (in degree) of the center point of the ith window, respectively; φ_U, λ_U, and h are the latitude (in degree), longitude (in degree) and height (in meter) of the target location, respectively; α_1 is the average value of T_m; α_2 is the latitude correction; α_3 is the height correction; and (α_4, α_5) and (α_6, α_7) are the amplitudes of annual and semi-annual periodicity, respectively. As shown in Eq. (11), these coefficients can be estimated by using the least square adjustment based on at least seven grid-point-specific data sets of each window. According to the factors determining window size as described in Sect. 3.1, in this work, we finally chose the size of the window as $5° \times 4°$ (lon. × lat.). The coefficients of GGTm, hence, are also expressed in the form of a $5° \times 4°$ (lon. × lat.) grid. Thus, we can divide the globe into 3240 regular windows (grid points).

Here, we introduce the use of GGTm. Users only need to provide the doy and target position and then find the nearest grid point between the target position and grid points of the model parameters based on the latitude and longitude of the target location. The T_m values at the target position can be calculated using the nearest gridded coefficients and Eq. (11).

3.3 Data source for establishing GGTm

The website of global geodetic observing system (GGOS) Atmosphere (a server at TU Vienna) can provide global atmospheric delay grid data (such as ZHD, ZWD and T_m) at a spatial resolution of $2.5° \times 2°$ (lon. × lat.) and with a temporal resolution of 6 h (at UTC 00:00, 06:00, 12:00 and 18:00) (http://ggosatm.hg.tuwien.ac.at). These global surface grid products are calculated from ECMWF reanalysis data and all correspond to the ellipsoidal heights; the global ellipsoidal height grid data are also provided by GGOS Atmosphere

with a spatial resolution of $2.5° \times 2°$ (lon. × lat.). Yao et al. (2014c) conducted an accuracy test for gridded T_m data using 341 globally distributed radiosonde sites; the results suggest that the gridded T_m data are highly reliable and precise and can be used as a data source for establishing the GGTm. In this work, the GGTm model parameters are estimated using gridded T_m data from 2007 to 2014 and global ellipsoidal height grid data based on the least square method. The parameters of GGTm are all stored in the form of a $5° \times 4°$ (lon. × lat.) grid over the globe.

4 Validation of GGTm

To assess the performance of the new GGTm model, we compared it to the widely used Bevis formula ($T_m = 70.2 + 0.72T_s$) and the newest release of the GPT2w model using the same reference T_m values derived from gridded T_m data and radiosonde profiles. The GPT2w model has two horizontal resolutions of $1° \times 1°$ and $5° \times 5°$. To describe them conveniently, we defined these two resolutions as GPT2w-1 and GPT2w-5, respectively. In this work, bias and root mean square error (RMS) were considered as the criteria for accuracy assessment and are calculated by the following equations:

$$
\mathrm{bias} = \frac{1}{N} \sum_{i=1}^{N} \left(T_m^{M_i} - T_m^{R_i}\right)
\tag{12}
$$

$$
\mathrm{RMS} = \sqrt{\frac{1}{N} \sum_{i=1}^{N} \left(T_m^{M_i} - T_m^{R_i}\right)^2}
\tag{13}
$$

where $T_m^{M_i}$ is the T_m value calculated by the model, $T_m^{R_i}$ is the reference T_m value derived from gridded T_m data or radiosonde profiles, and N is the number of samples.

4.1 Comparison to gridded T_m data

In this section, for the global gridded T_m data from 2015, there are a total of 13,195 T_m grids, and these are used as the reference values to assess the four models. The global gridded T_m data with a temporal resolution of 6 h (at UTC 00:00, 06:00, 12:00 and 18:00) and the T_m of each grid point at the same time are calculated using the GGTm, GPT2w-1, GPT2w-5 and Bevis models; thus, the daily bias and RMS can be obtained for these models. For the Bevis formula ($T_m = 70.2 + 0.72T_s$), the T_s measurements are unavailable in oceanic areas. The T_s value can thus be derived from empirical GPT series models (Böhm et al. 2007, 2015). Here, we regard the gridded T_m data from 2015 as the reference values to analyze the impact of T_s values calculated from the GPT, GPT2w-5 and GPT2w-1 models on the Bevis formula. The

Table 1 Statistical results of the impact of T_s derived from the GPT, GPT2w-5 and GPT2w-1 models on Bevis formula calculation using gridded T_m data from 2015

Model	Bevis&GPT	Bevis&GPT2w-5	Bevis&GPT2w-1
bias (in K)			
Max.	14.60	18.70	13.58
Min.	− 6.60	− 6.68	− 7.25
Mean	1.18	1.17	1.16
RMS (in K)			
Max.	15.50	19.49	14.23
Min.	1.23	1.33	1.32
Mean	4.85	4.76	4.74

Table 2 Statistical results of different models validated by using gridded T_m data from 2015

Model	Bevis+GPT2w-1	GPT2w-5	GPT2w-1	GGTm
bias (in K)				
Max.	13.58	24.68	11.93	3.48
Min.	− 7.25	− 13.52	− 3.19	− 2.24
Mean	1.16	0.01	0.02	− 0.05
RMS (in K)				
Max.	14.23	24.98	12.43	5.67
Min.	1.32	1.02	1.02	0.86
Mean	4.74	3.43	3.29	2.89

statistical results of the bias and RMS of different models in 2015 are shown in Table 1.

Table 1 shows that both the bias and RMS of T_m derived from Bevis&GPT2w-1 are the smallest; thus, GPT2w-1 can provide the most precise T_s value for the Bevis formula compared to that of the other two models. Therefore, we chose the T_s derived from GPT2w-1 for the calculation of the Bevis formula. As previously described, the estimated T_m values from these models are compared to the gridded T_m data. The statistical results of the bias and RMS of the different models tested by gridded T_m data in 2015 are shown in Table 2 and Fig. 2.

Table 2 shows that for GGTm, the bias is − 0.05 K and ranges from − 2.24 to 3.48 K; the RMS is 2.89 K and ranges from 0.86 to 5.67 K. In terms of RMS, GGTm performs an approximately 0.5 K (16%) and 0.4 K (12%) improvement against GPT2w-5 and GPT2w-1 over the globe, respectively; GPT2w-1 shows slightly better than GPT2w-5, while the Bevis formula shows the largest RMS value. Figure 2 reflects larger errors in parts of western China, the Himalayas, Antarctic areas, Chile, Peru and Greenland for the GPT2w-5. Relative to GPT2w-5, GPT2w-1 improves the spatial resolution of the model parameters, larger errors are still observed in parts of Greenland, Chile, western China and the Antarctic, which are mainly affected by the complex topography because GPT2w does not take the height variation of T_m into account. While the GGTm shows stable and accurate results in T_m estimation over the globe. Therefore, GGTm significantly outperforms GPT2w in these areas with great undulating terrain. For the Bevis formula, it shows strong negative bias in low latitudes and positive bias in the Antarctic regions; similarly, a larger RMS exists in parts of Greenland and western China, especially south of 60°S latitude toward the Antarctic region and parts of the oceanic areas. The Bevis formula only uses radiosonde profiles in North America for modeling. In addition, the Bevis formula does not consider the vertical lapse of T_m, which results in a worse performance when used in these areas. In all, GGTm shows significant

superiority against other models and is without large error in estimating T_m on a global scale.

To analyze the stability and accuracy of different models on different days of the year (DOY), the daily bias and RMS at all grids of each model were statistically analyzed, and the results varied with DOY as shown in Fig. 3.

From Fig. 3, the Bevis formula shows significant positive bias all year, larger bias and RMS values are observed during both the spring and autumn months, and it has the largest bias and RMS among all the models. The other three models show obvious negative bias during both spring and winter days and positive bias during summer days, while for the RMS, these three models are without obvious seasonal variation. In all, the GGTm shows the best accuracy (in terms of RMS) during the whole year-long period.

4.2 Comparison to radiosonde data

A total of 412 globally distributed radiosonde stations are selected. The distribution of the selected radiosonde stations is shown in Fig. 4. There are more radiosonde stations distributed in the Northern Hemisphere than there are in the Southern Hemisphere. As described in Sect. 2.1, the T_m values computed from radiosonde profiles using the integration method at UTC 00:00 and 12:00 every day in 2015 are treated as the reference values to validate the new GGTm, GPT2w-5, GPT2w-1 and Bevis $T_m − T_s$ formula (T_s is in situ surface temperature derived from the radiosonde site). All the 412 selected radiosonde stations contain available data of over half of the year (the abnormal radiosonde profiles are removed) to ensure the reliability of validation. The statistical results of bias and RMS of the different models are shown in Table 3 and Fig. 5.

From Table 3, the Bevis formula has the largest RMS of 4.10 K and the smallest absolute bias of 0.02 K. The RMS is 4.03 K for GPT2w-5 and 3.82 K for GPT2w-1. Both the largest negative bias and RMS are observed for GPT2w-5, meaning that GPT2w-1 shows relative stable values than
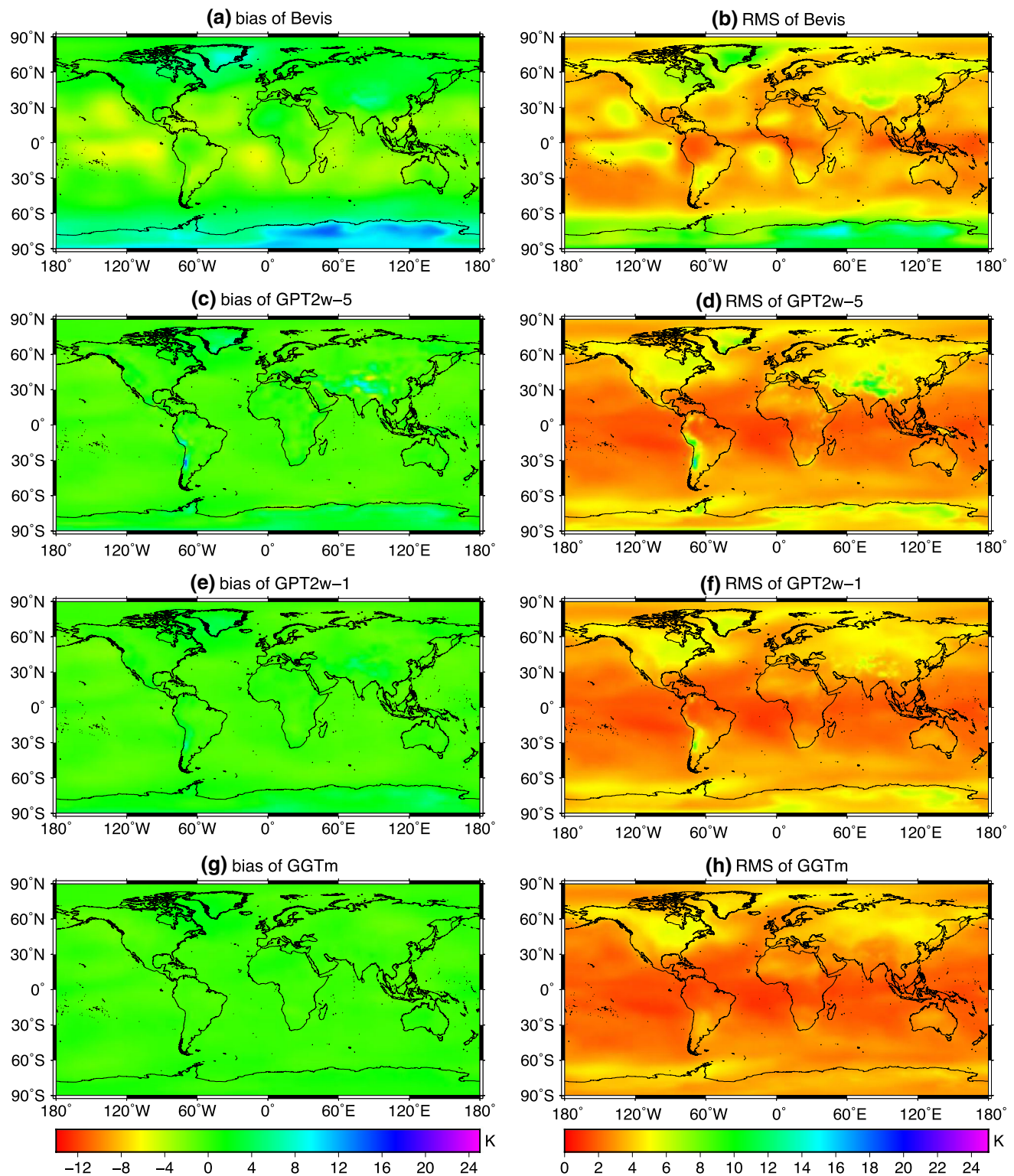
Fig. 2 Global distribution of bias and RMS in different models tested by using gridded T_m data from 2015

those of GPT2w-5 through improving the spatial resolution of the model. GGTm has the smallest RMS of 3.54 K and ranges from 1.14 to 6.90 K, which performs an approxi-

mately 0.5 K (12%) and 0.3 K (8%) improvement against both GPT2w-5 and GPT2w-1 over the globe, respectively. Therefore, GGTm shows excellent performance against other
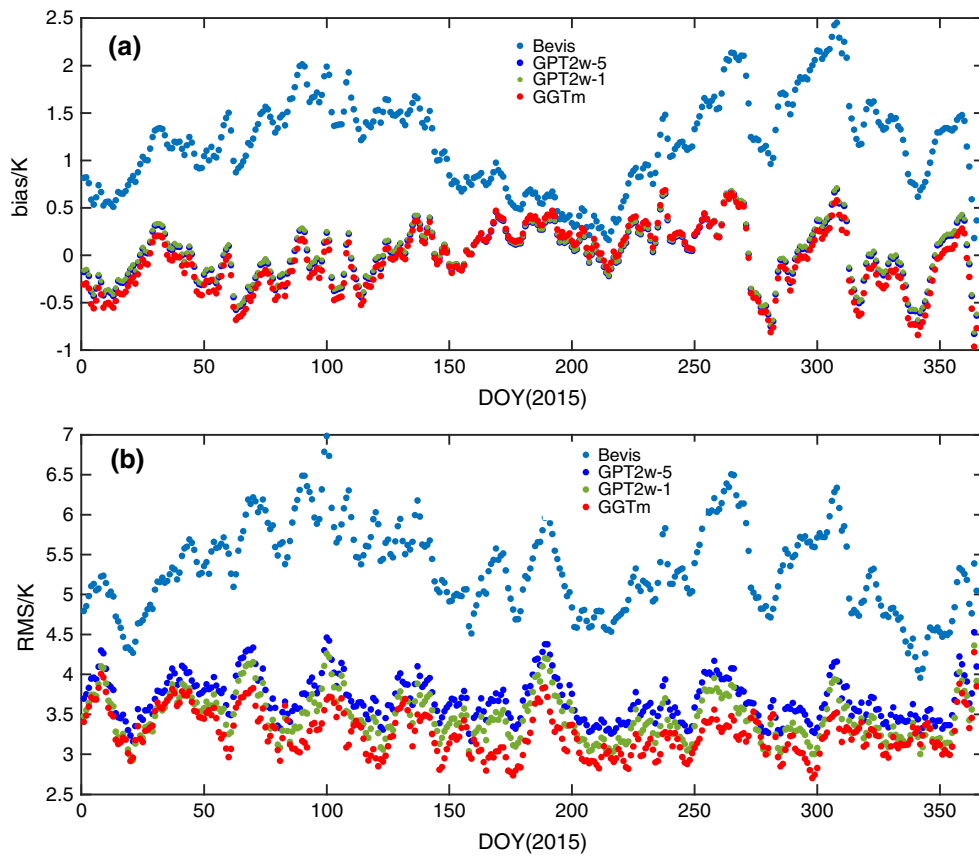
Fig. 3 Results of different models tested by gridded T_m data during different days of the year
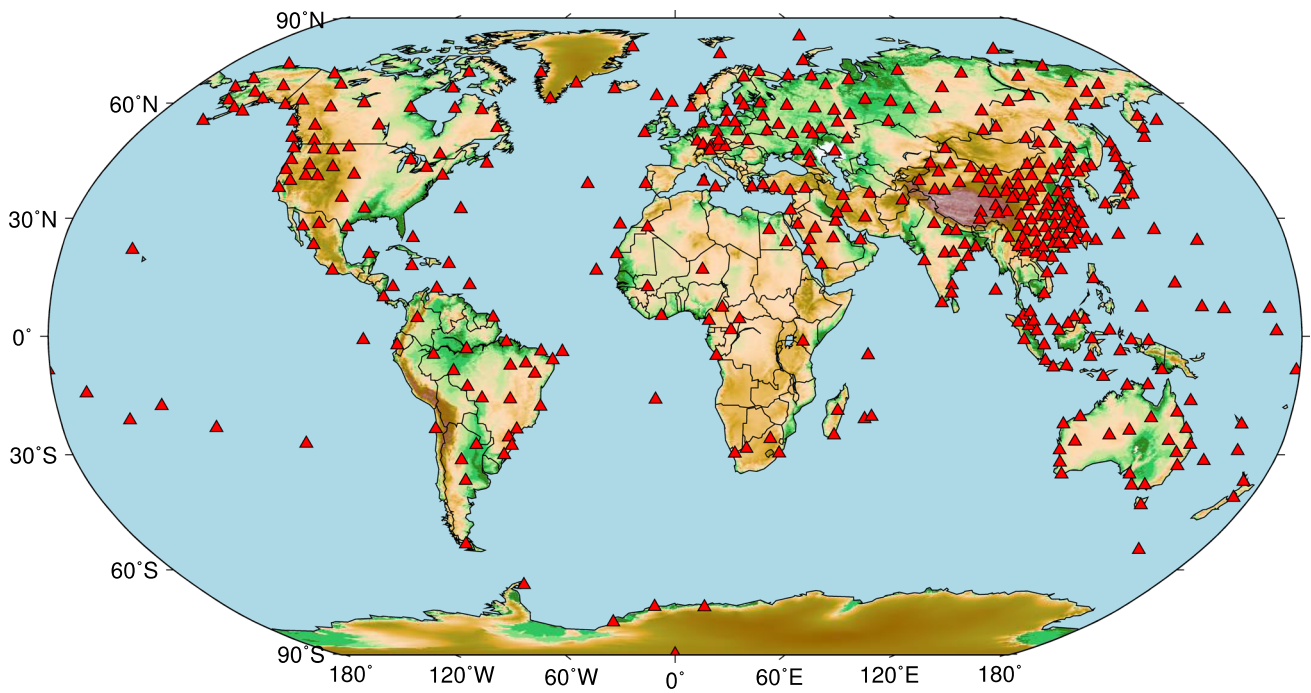
Fig. 4 Global distribution of selected 412 radiosonde stations for the validation of GGTm

Table 3 Statistical results of different models validated using radiosonde data from 2015

Model	Bevis	GPT2w-5	GPT2w-1	GGTm
bias (in K)				
Max.	7.75	8.39	4.49	3.61
Min.	− 6.12	− 13.89	− 6.63	− 3.67
Mean	− 0.02	− 0.93	− 0.76	0.03
RMS (in K)				
Max.	8.33	14.42	8.44	6.90
Min.	1.32	1.45	1.48	1.14
Mean	4.10	4.03	3.82	3.54

models over the globe. Figure 5 shows that all of these models can achieve relatively high accuracy (in terms of RMS) over low latitude areas; the reasons for this will be analyzed later. The Bevis formula shows an obvious cold bias in low latitudes and a warm bias in Russia as well as western areas of China, but it presents relatively high accuracy in North American areas, where the radiosonde sites are more involved in the Bevis modeling. For GPT2w-5, both larger bias and RMS are observed in parts of Northwest China and Chile. In addition, both GPT2w-5 and GPT2w-1 show larger cold bias in parts of Northwest China and western North America; relative to GGTm, GPT2w-1 still shows larger RMS values in parts of Northwest China and Northwest South America. While for GGTm, both bias and RMS are small and stable on a global scale. Additionally, the results of bias and RMS at all selected radiosonde sites of each model were further statistically analyzed, and the error distribution and statistics of the different models are shown in Figs. 6 and 7.

Figure 6 shows that the bias of GGTm is highly concentrated around zero; although the bias of the Bevis formula is relatively concentrated around zero, the number of strong negative biases is approximately equal to the number of positive biases, resulting in a small mean bias, while the biases of both GPT2w-5 and GPT2w-1 are relatively scattered (most are negative biases), which indicates that the T_m derived from the GPT2w model has few systematic deviations compared to those of the radiosonde data. From Fig. 7, we can see more intuitively that the RMS of the Bevis formula comprises 77% below 5 K and only 21% below 3 K, and it has a large proportion (7%) over 6 K. For GPT2w-5, the RMS comprises 78% (83% for GPT2w-1) below 5 K and only 26% (28% for GPT2w-1) below 3 K, and the proportion over 6 K is higher than that of GPT2w-1, but the proportion below 2 K is slightly greater than that of GPT2w-1, while the RMS of GGTm accounts for the both the largest proportion of below 5 K (90%) and below 3 K (32%) among the four models. For the proportion of below 5 K, that of GGTm increased by 12 and 7% over GPT2w-5 and GPT2w-1, respectively, while for the proportion of below 3 K, that of GGTm increased

by 6 and 4% over GPT2w-5 and GPT2w-1, respectively. In addition, GGTm has the smallest proportion over 6 K (2%) and the largest proportion below 2 K (11%). For the proportion of over 6 K, that of GGTm decreased by 5 and 2% over GPT2w-5 and GPT2w-1, respectively, while for the proportion of below 2 K, that of GGTm increased by 3 and 5% over GPT2w-5 and GPT2w-1, respectively. Therefore, it further illustrated that the GGTm model performs excellent performance against other models over the globe.

To analyze the bias and RMS of the seasonal variations in different models, the daily results at all selected stations of each model were statistically analyzed, and the bias and RMS values of different models varying with DOY are shown in Fig. 8.

From Fig. 8, the biases of GGTm are generally the smallest and without obvious seasonal variation. Both GPT2w-5 and GPT2w-1 show negative bias during most DOY, and relatively strong negative bias existed during spring and winter days, further indicating that the T_m calculated from the GPT2w model has some systematic errors, while the Bevis formula shows obvious positive bias during the spring and negative bias during the summer. In terms of RMS, all of these models have obvious seasonal variations, which show relative larger RMS values during the spring and winter and smaller RMS values during summer days. Because most of the selected radiosonde stations are in the middle and high latitudes of the Northern Hemisphere, T_m changes are small during the summer and larger during the winter. The GGTm shows the highest accuracy and stability during the whole year period. For the other models, however, the stability and accuracy of the models vary at different DOY. To further illustrate the performance of the GGTm model in terms of the seasonal variation, the results of the monthly bias and RMS in different models are shown in Fig. 9.

From Fig. 9a, one can see that both GPT2w-5 and GPT2w-1 present larger negative monthly bias among 12 months, while GGTm shows a stable and smaller monthly bias. From January to June as well as October to December, GGTm performs significant advantages against both GPT2w-5 and GPT2w-1 in terms of monthly bias. Figure 9b shows that the GGTm still has excellent performance against other models in terms of monthly RMS. GGTm performs an approximately 0.5 and 0.3 K improvement over the GPT2w-5 and GPT2w-1, respectively. Therefore, GGTm performs excellent performance over other models in terms of the monthly or seasonal variation.

The T_m has strong correlations with both altitude and latitude. To investigate the relations between altitude and the bias and RMS, 412 radiosonde stations were sorted into six categories based on altitude, i.e., lower than 500, 500–1000, 1000–1500, 1500–2000, 2000–2500, and above 2500 m. The results of the bias and RMS in each altitude range are shown in Fig. 10.
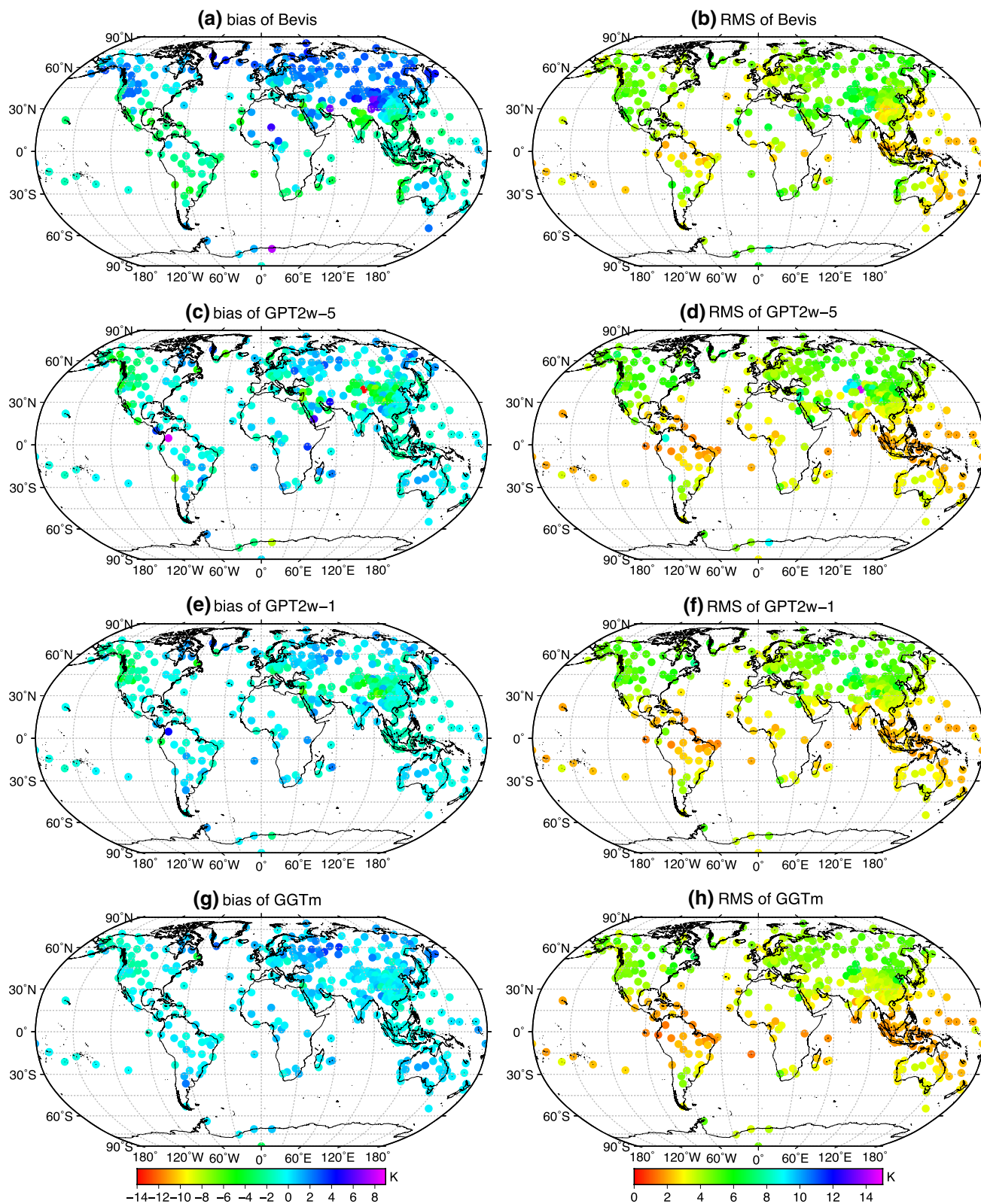
Fig. 5 Global distribution of bias and RMS of different models tested using radiosonde data from 2015
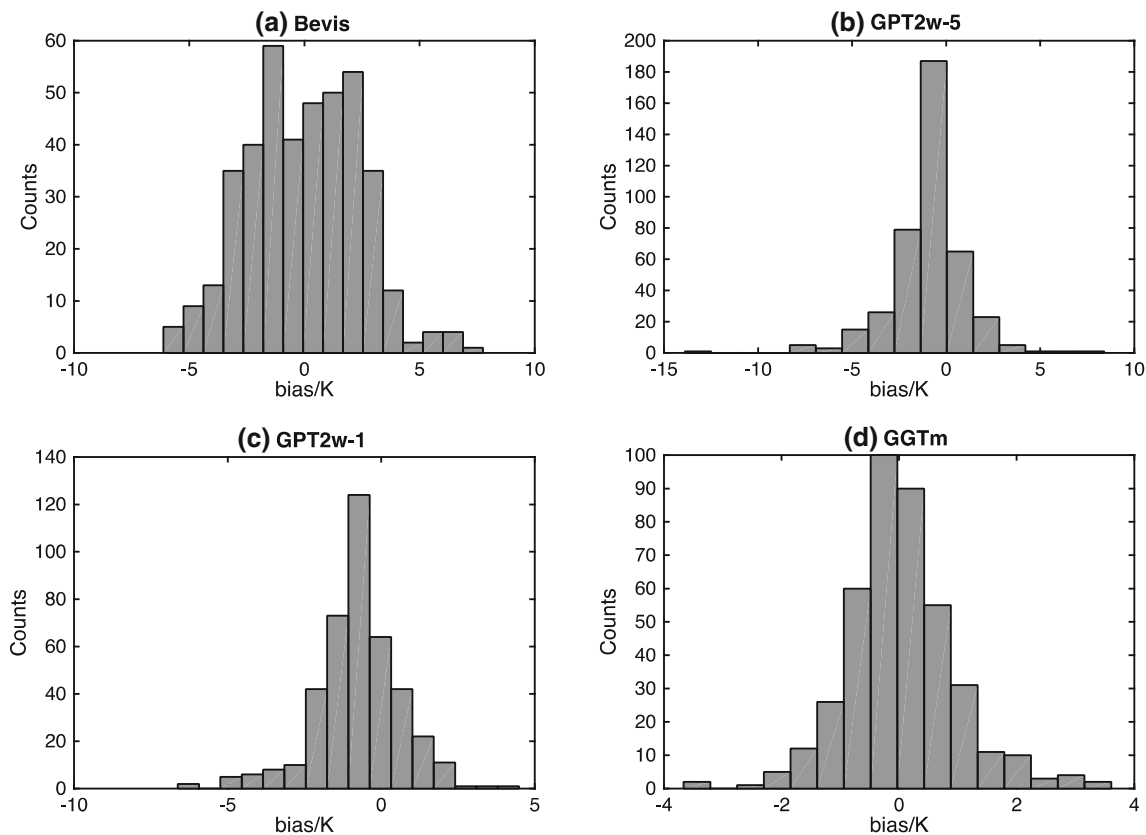
Fig. 6 Histogram of bias of different models tested by using radiosonde data from 2015

Figure 10 shows that in general, both the bias and RMS increase with increasing altitude in the Bevis formula; although those of both GPT2w-5 and GPT2w-1 are not obvious, larger bias and RMS still existed in high-altitude areas for GPT2w-5 and GPT2w-1. The GGTm significantly outperforms all the other models in high-altitude areas, especially in the areas with altitude of above 2500 m, which performs an approximately 2.5, 1.3 and 1.2 K improvement (in terms of RMS) over the Bevis formula, GPT2w-5 and GPT2w-1, respectively. In contrast, the GGTm has both the smallest bias and RMS in each altitude range and small differences among them at different altitude ranges, verifying excellent performance of the GGTm as compared to that of the other three models.

Furthermore, the relations between latitude and the bias and RMS values in different models were analyzed. To visualize the variation in the bias and RMS, 412 radiosonde stations were sorted in terms of latitude in 15° intervals. The results are shown in Fig. 11.

From Fig. 11, one can see that the Bevis formula has both relatively larger bias and RMS at most of the latitude ranges, and the bias of the Bevis formula increases with increasing latitude in the Northern Hemisphere. In addition, the Bevis formula, GPT2w-5 and GPT2w-1 show obvious negative

biases at low and middle latitudes, especially in the high-latitude areas of the Southern Hemisphere, where larger bias and RMS were observed for Bevis formula and GPT2w-5. The accuracy (in terms of RMS) of the Bevis formula at middle latitudes (30°N−60°N) in the Northern Hemisphere is slightly higher than that of both GPT2w-5 and GPT2w-1. These results reflect the advantage of the Bevis formula in those regions where the radiosonde data are involved in the modeling. The best performance of all models is obtained at low latitudes (30°S−30°N), where the amplitudes of T_m are much smaller than those at high latitudes (Yao et al. 2014b). However, the GGTm performs excellent performance against other models in the areas with the latitude range from 15°S to 45°N. In all, GGTm shows best accuracy and stability over other models.

4.3 Impact of T_m on GPS-PWV

In GPS meteorology, the goal of determining T_m is to map the ZWD onto GPS-PWV. Most of the GPS stations are not equipped with meteorological sensors as the initial purpose of these was mainly for space geodetic studies. In addition, the GPS stations and radiosonde stations are not co-located,
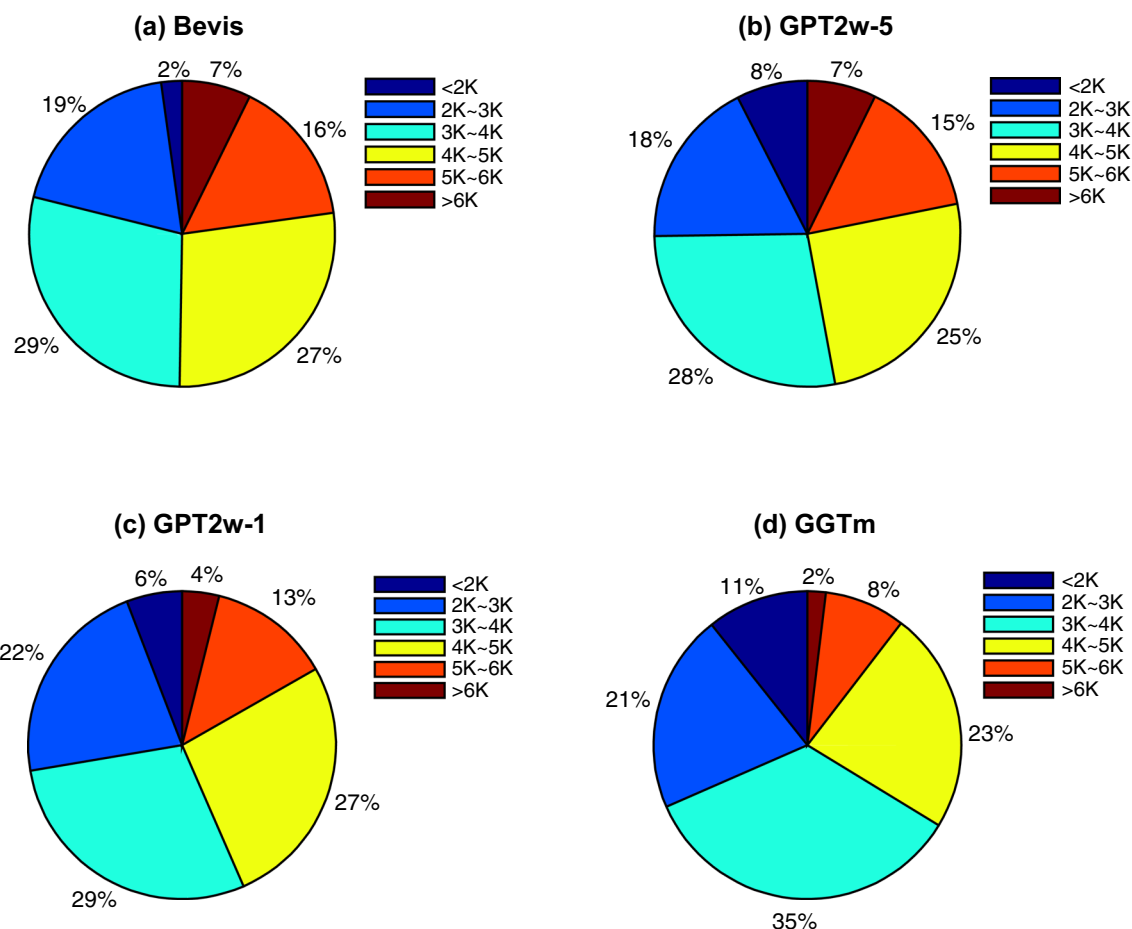
(a) Bevis

(b) GPT2w-5

(c) GPT2w-1

(d) GGTm

Fig. 7 Proportional distribution of RMS values of different models tested using radiosonde data from 2015

and thus, it is difficult to make a comprehensive and global assessment of the impact of T_m on GPS-PWV. Several investigations have been conducted to analyze the impact of T_m on its resultant GPS-PWV in terms of theoretical function (Wang et al. 2005, 2016; He et al. 2017). In this paper, a similar method is employed to analyze the impact of T_m on GPS-PWV, and the commonly used relationship of the RMS between T_m and PWV can be calculated using the following:

$$\frac{\text{RMS}_{\text{PWV}}}{\text{PWV}} = \frac{\text{RMS}_{\Pi}}{\Pi} = \frac{k_3 \text{RMS}_{T_m}}{\left(\frac{k_3}{T_m} + k_2'\right) T_m^2}$$

$$= \frac{k_3}{\left(\frac{k_3}{T_m} + k_2'\right) T_m} \cdot \frac{\text{RMS}_{T_m}}{T_m} \tag{14}$$

where RMS_{PWV} is the error in PWV, RMS_{T_m} is the error in T_m achieved from Sect. 4.2, PWV and T_m are set to annual mean values and are also obtained from Sect. 4.2, RMS_{PWV}/PWV is defined as the relative error of PWV, and RMS_{PWV} and RMS_{PWV}/PWV are used to evaluate the impact of the errors in T_m on its resultant GPS-PWV. Some radiosonde stations with insufficient PWV data have been removed; finally, the

403 globally distributed radiosonde stations are selected. The global distributions of the theoretical results of RMS_{PWV} and RMS_{PWV}/PWV in different models are shown in Figs. 12 and 13 and Table 4.

Figure 12 shows the global distribution of RMS_{PWV} in 2015. The four models all show smaller RMS_{PWV} in both the Antarctic and Arctic regions, where the annual mean values of PWV are only approximately 3.0 and 8.0 mm in our experiment, respectively. According to Eq. (14), smaller annual mean RMS_{PWV} values can be achieved, although the smaller annual mean values of T_m are also observed in these regions (approximately 255 and 260 K, respectively). For the Bevis and GPT2w-5 models, the larger RMS_{PWV} values are observed at low latitudes (30°S−30°N), especially in parts of Southern Asia for the Bevis formula, where it has the largest RMS_{PWV} value of approximately 1.0 mm. At these low latitudes, both the largest annual mean PWV and T_m values of approximately 37.3 mm and 286 K occur for those two models in our experiment, respectively; similarly, though the smaller annual mean RMS values of T_m are obtained (described in Sect. 4.2) in these areas, there still resulting in larger annual mean RMS_{PWV} values as a contri-
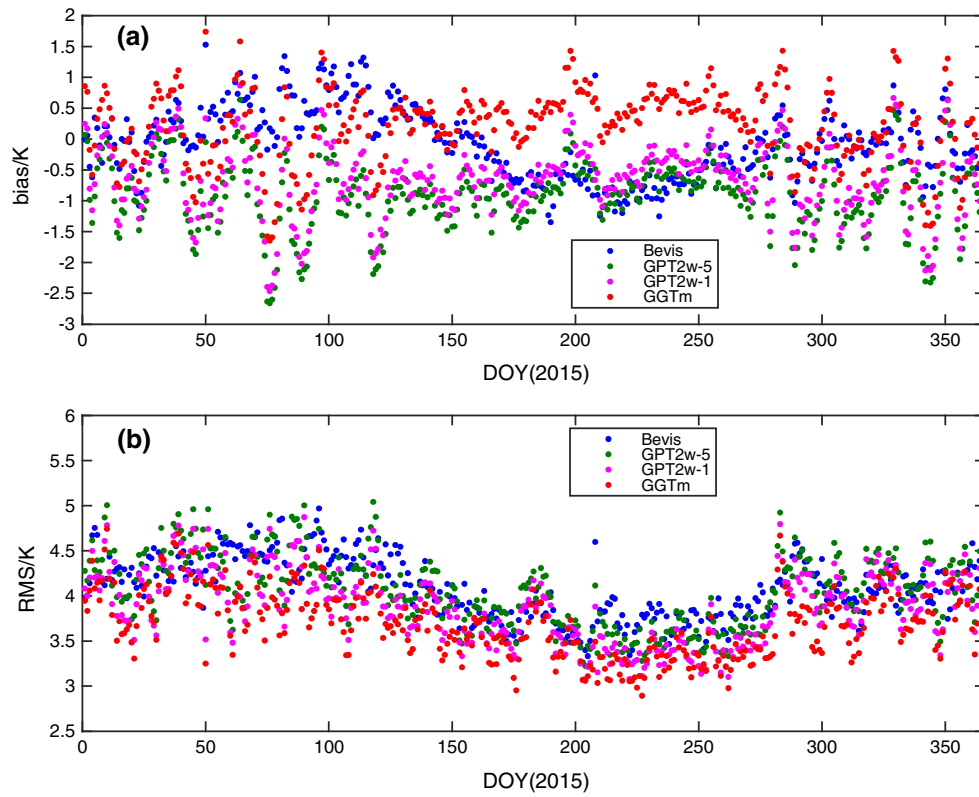
Fig. 8 Results of different models tested using radiosonde data during different days of the year
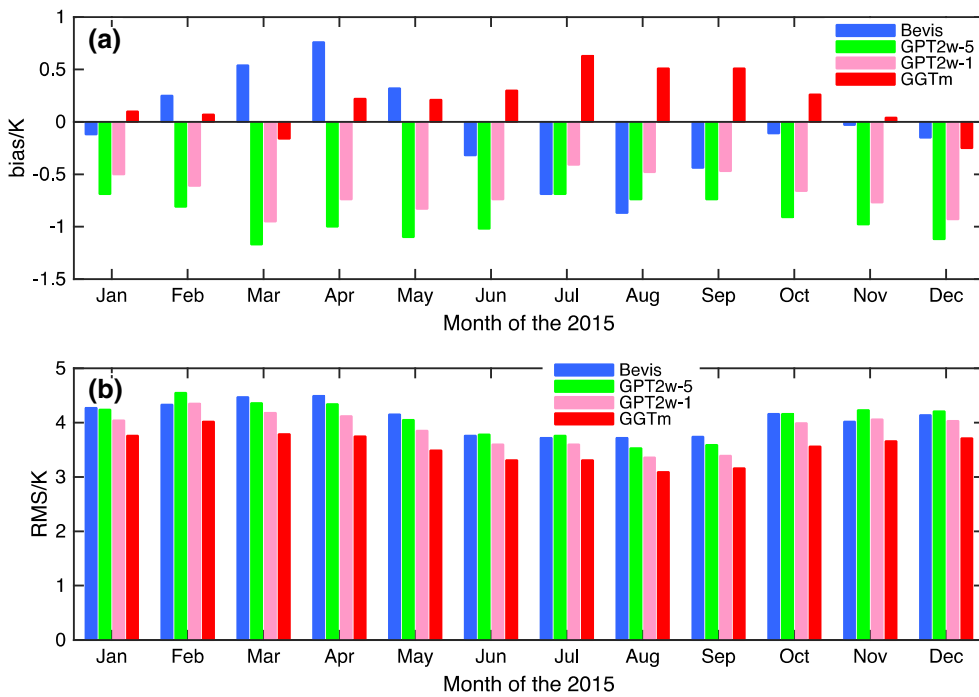

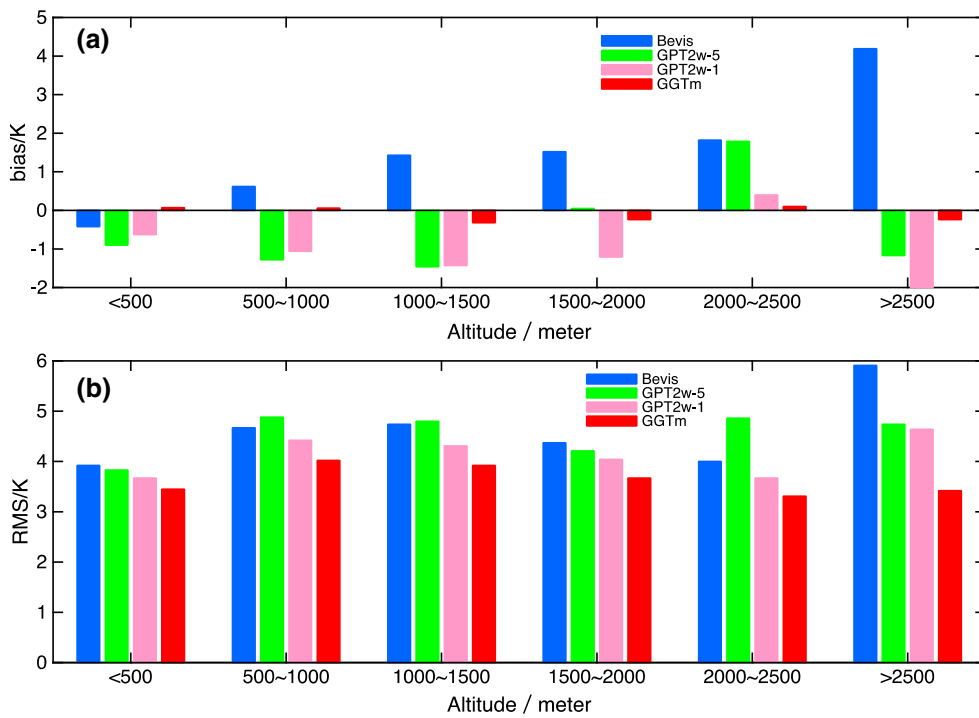**Fig. 9** Monthly performance of different models tested using radiosonde data

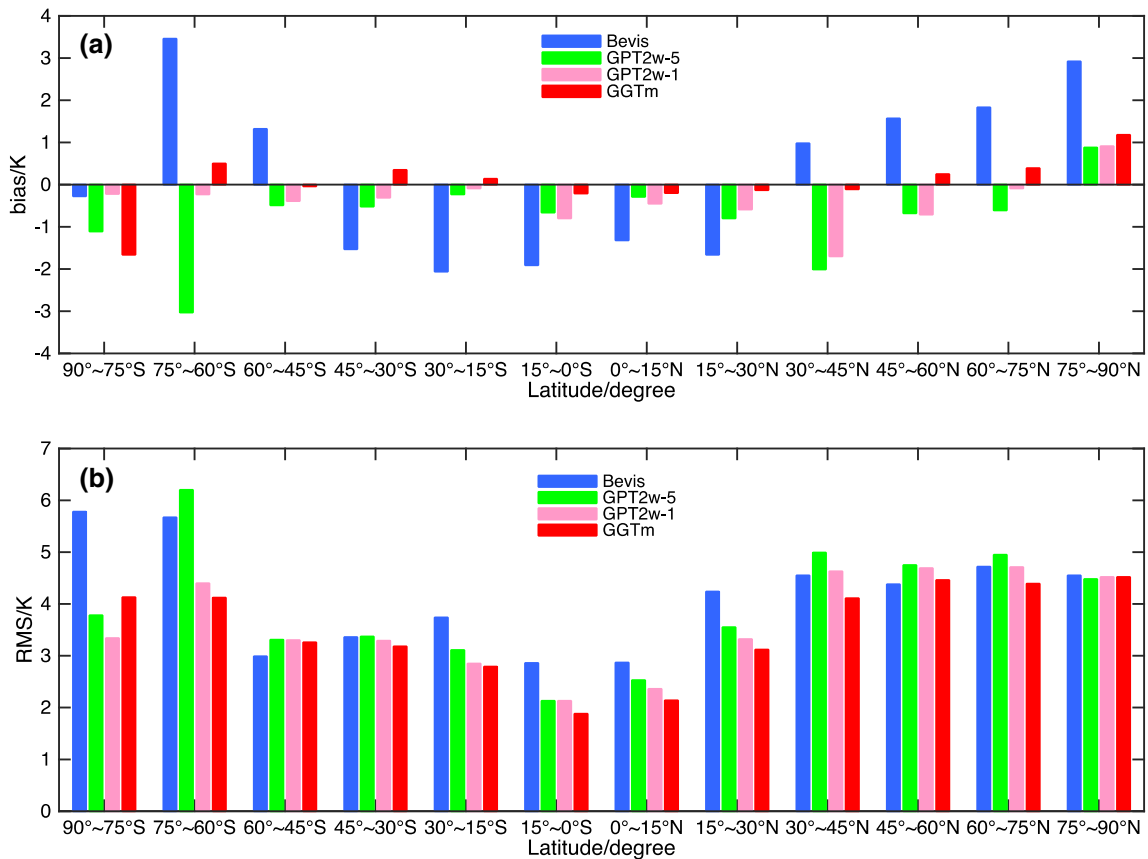**Fig. 10** Results of bias and RMS of the different models at different altitude ranges

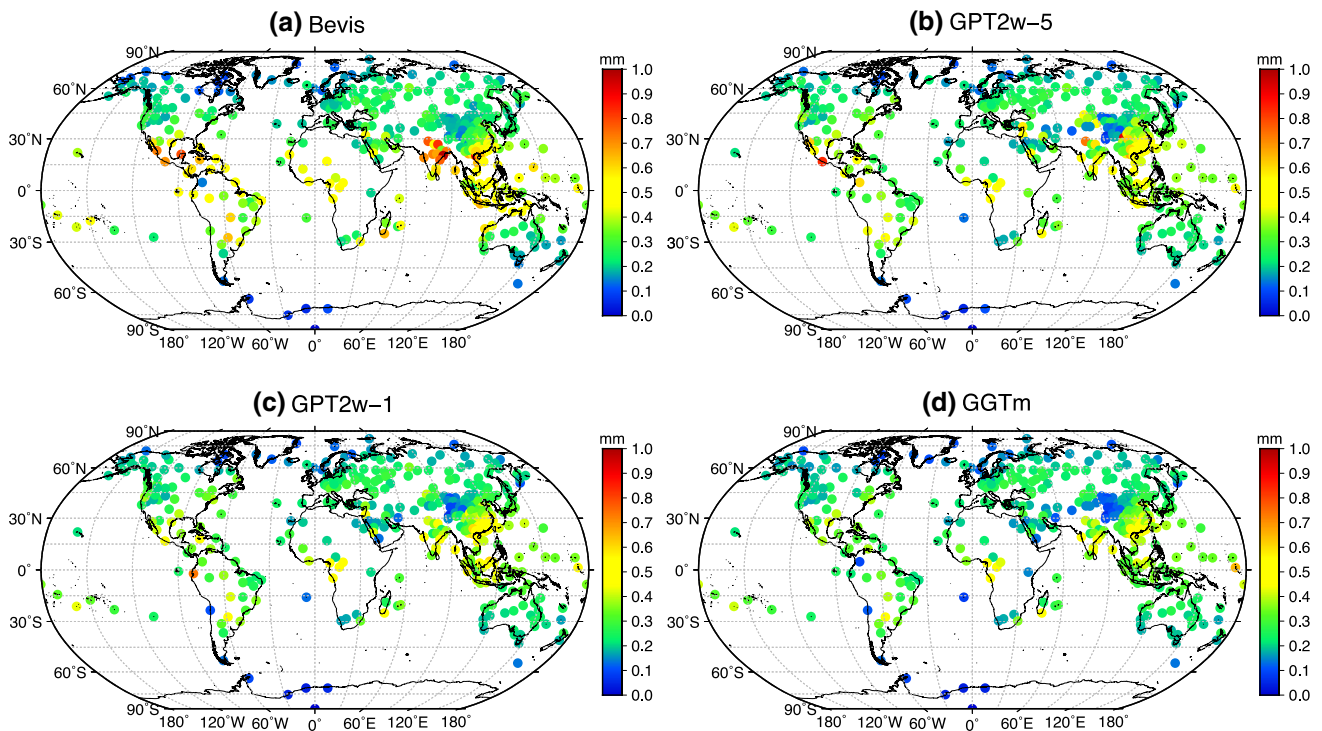**Fig. 11** Results of bias and RMS of different models at different latitude ranges

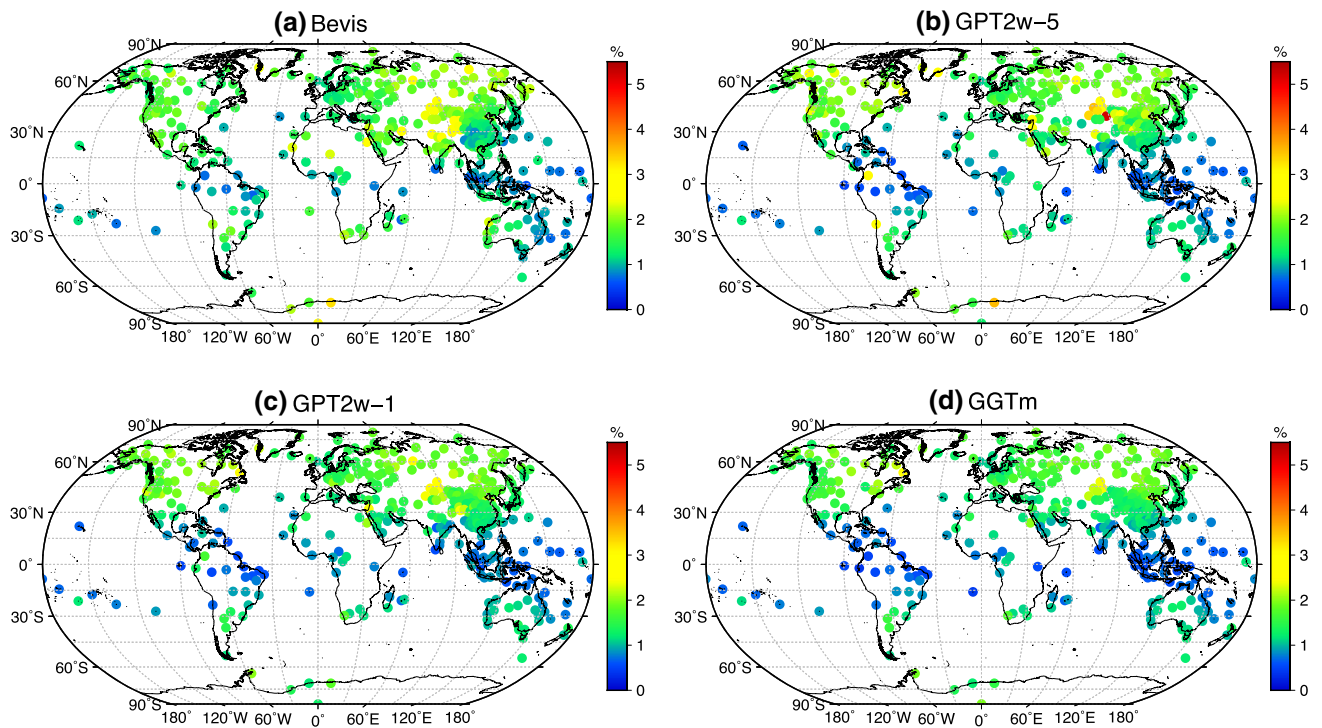**Fig. 12** The theoretical RMS of PWV resulting from different models using radiosonde data from 2015

Fig. 13 The theoretical relative error of PWV resulting from different models using radiosonde data from 2015

bution of larger PWV values. In contrast, for the GPT2w-1 and GGTm models, which show relatively smaller annual mean RMS_{PWV} values. From Fig. 13, one can see that the

GGTm, GPT2w-5 and GPT2w-1 models all show smaller RMS_{PWV}/PWV at low latitudes, especially from south of 15° latitude to the north of 15° latitude, where the Bevis formula

Table 4 Statistical results of theoretical RMS and relative error of PWV resulting from different models validated by using radiosonde data from 2015

	RMS_{PWV} (mm)			RMS_{PWV}/PWV (%)		
	Max.	Min.	Mean	Max.	Min.	Mean
Bevis	0.99	0.01	0.31	3.28	0.45	1.47
GPT2w-5	0.92	0.01	0.30	5.20	0.50	1.46
GPT2w-1	0.74	0.01	0.28	3.06	0.51	1.38
GGTm	0.65	0.01	0.26	2.53	0.40	1.28

shows relatively larger RMS_{PWV}/PWV than that of the other three models. The smallest RMS of T_m and the largest T_m values are obtained in these regions, resulting in the smaller annual mean RMS_{PWV}/PWV values. For the Bevis formula, GPT2w-5 and GPT2w-1, relatively larger RMS_{PWV}/PWV values are still observed in parts of western China, while GGTm shows relative stable performance over the globe. From Table 4, the RMS_{PWV} values of the GGTm are less than 0.65 mm and with a global mean RMS_{PWV} value of 0.26 mm; in terms of RMS_{PWV}/PWV, GGTm has a global mean value of 1.28% and ranges from 0.40 to 2.53%. As the GGTm is an empirical global model, which can provide an accurate Tm values for retrieving accurate real-time PWV. Thus, GGTm has possible potential applications in the real-time analysis or nowcasting of severe weather conditions such as heavy rainfall, flood, and typhoon events, especially for the application of low-latitude areas and western China.

5 Conclusions

T_m is a crucial parameter for detecting GPS-PWV. A reliable and accurate T_m empirical model is needed for the application of real-time PWV sounding, especially when in situ meteorological observations are unavailable. T_m shows significant season and location dependence on a global scale. The existing T_m empirical models do not completely account for variations in both altitude and latitude. In this research, both latitude and altitude variations were considered in the modeling, and a new global grid T_m model, namely GGTm, was developed based on a sliding window algorithm using global gridded T_m data and global ellipsoidal height grid data.

The accuracy and stability of the GGTm were validated using global gridded T_m data and globally distributed radiosonde station data from 2015, and detailed comparisons to the Bevis, GPT2w-5 and GPT2w-1 models were also conducted. GGTm shows significant accuracy and stability among the four models over the globe when compared using global gridded T_m data, especially in the areas with highly undulating terrain, while the Bevis formula shows the worst results and obvious systematic bias. When compared

using radiosonde data, GGTm still maintained excellent performance against other models, with an annual mean bias and RMS of 0.03 and 3.54 K, respectively. GPT2w-1 showed slightly better performance than GPT2w-5, but both models had significant systematic bias, especially in high-altitude areas due to the GPT2w does not take the height variation of T_m into account, while the Bevis formula still presented the worst result. Additionally, the impact of T_m on GPS-PWV was analyzed, showing that the global mean values of RMS_{PWV} and RMS_{PWV}/PWV are 0.26 mm and 1.28% for GGTm, respectively.

In this experiment, the Bevis formula and GPT2w models show a relatively poorer ability to calculate the T_m in high-altitude areas, as both models do not consider the altitude variation in modeling; GPT2w-1, to a certain extent, can mitigate this effect by improving the spatial resolution of model parameters, but larger errors are still existed in the areas with the altitude of above 2500 m. GGTm has the ability to provide excellent accurate and reliable T_m value over the globe and requires no in situ meteorological parameters as inputs, making the GGTm model more powerful and practical for calculating T_m, and it will have wide applicability in real-time GPS-PWV sounding, especially for the application of low-latitude areas and western China. In future work, we will mainly focus on considering diurnal variation in the model, analyzing the impact of the window size on the model, and combining multi-source data in the modeling.

References

Adams DK, Gutman SI, Holub KL, Pereira DS (2013) GNSS observations of deep convective time scales in the Amazon. Geophys Res Lett 40:2818–2823

Askne J, Nordius H (1987) Estimation of tropospheric delay for microwaves from surface weather data. Radio Sci 22:379–386

Bevis M, Businger S, Chiswell S, Herring TA, Rocken C, Anthes RA, Ware RH (1992) GPS meteorology: remote sensing of atmospheric water vapor using the global positioning system. J Geophys Res 97(D14):15787–15801

Bevis M, Businger S, Chiswell S, Herring TA, Anthes RA, Rocken C, Ware RH (1994) GPS meteorology: mapping zenith wet delays onto precipitable. J Appl Meteorol 33:379–386

Böhm J, Heinkelmann R, Schuh H (2007) Short note: a global model of pressure and temperature for geodetic applications. J Geod 81(10):679–683

Böhm J, Moller G, Schindelegger M, Pain G, Weber R (2015) Development of an improved empirical model for slant delays in the troposphere (GPT2w). GPS Solut 19:433–441

Bolton D (1980) The computation of equivalent potential temperature. Mon Weather Rev 108:1046–1053

Byun SH, Bar-Sever YE (2009) A new type of troposphere zenith path delay product of the international GNSS service. J Geod 83:367–373

Chen P, Yao WQ, Zhu XJ (2014) Realization of global empirical model for mapping zenith wet delays onto precipitable water using NCEP re-analysis data. Geophys J Int 198:1748–1757

Emardson TR, Derks HJP (2000) On the relation between the wet delay and the integrated precipitable water vapour in the European atmosphere. Meteorol Appl 7:61–68

Emardson TR, Elgered G, Johansson JM (1998) Three months of continuous monitoring of atmospheric water vapor with a network of global positioning system receivers. J Geophys Res 103(D2):1807–1820

He CY, Wu SQ, Wang XM, Hu AD, Wang QX, Zhang KF (2017) A new voxel-based model for the determination of atmospheric weighted mean temperature in GPS atmospheric sounding. Atmos Meas Tech 10:2045–2060

Hobiger T, Ichikawa R, Takasu T, Koyama Y, Kondo T (2008a) Ray-traced troposphere slant delays for precise point positioning. Earth Planets Space 60(5):e1–e4

Hobiger T, Ichikawa R, Koyama Y, Kondo T (2008b) Fast and accurate ray-tracing algorithms for real-time space geodetic applications using numerical weather models. J Geophys Res 113:D20302. https://doi.org/10.1029/2008JD010503

Huelsing HK, Wang JH, Mears C, Braun JJ (2017) Precipitable water characteristics during the 2013 Colorado flood using ground-based GPS measurements. Atmos Meas Tech 10:4055–4066

Jin SG, Luo OF (2009) Variability and climatology of PWV from global 13-year GPS observations. IEEE T Geosci Remote Sens 47:1918–1924

Li JG, Mao JT, Li CC (1999) The approach to remote sensing of water vapor based on GPS linear regression T_m in eastern region of China. Acta Meteorol Sin 57(3):283–292

Lu CX, Zus F, Ge MR, Heinkelmann R, Dick G, Wickert J, Schuh H (2016) Tropospheric delay parameters from numerical weather models for multi-GNSS precise positioning. Atmos Meas Tech 9:5965–5973. https://doi.org/10.5194/amt-9-5965-2016

Lu CX, Li XX, Zus F, Heinkelmann R, Dick G, Ge MR, Wickert J, Schuh H (2017) Improving BeiDou real-time precise point positioning with numerical weather models. J Geod 91:1019–1029. https://doi.org/10.1007/s00190-017-1005-2

Ross RJ, Rosenfeld S (1997) Estimating mean weighted temperature of the atmosphere for Global Positioning System applications. J Geophys Res Atmos 102:21719–21730

Sapucci LF, Machado LAT, Menezes de Souza E, Campos TB (2016) GPS-PWV jumps before intense rain events. Atmos Meas Tech Discuss. https://doi.org/10.5194/amt-2016-378

Wang JH, Zhang LY (2009) Climate applications of a global, 2-hourly atmospheric precipitable water dataset derived from IGS tropospheric products. J Geod 83(3–4):209–217

Wang JH, Zhang LY, Dai AG (2005) Global estimates of water-vapor-weighted mean temperature of the atmosphere for GPS applications. J Geophys Res. https://doi.org/10.1029/2005JD006215

Wang JH, Zhang LY, Dai AG, Van Hove T, Van Baelen J (2007) A near-global, 2-hourly data set of atmospheric precipitable water from ground-based GPS measurements. J Geophys Res Atmos. https://doi.org/10.1029/2006JD007529

Wang XY, Dai ZQ, Cao YC, Song LC (2011) Weighted mean temperature T_m statistical analysis in ground-based GPS in China. Geomat Inform Sci Wuhan Univ 36(4):412–416

Wang XM, Zhang KF, Wu SQ, Fan SJ, Cheng YY (2016) Water vapor-weighted mean temperature and its impact on the determination of precipitable water vapor and its linear trend. J Geophys Res Atmos 121:833–852

Yao YB, Zhu S, Yue SQ (2012) A globally applicable, season-specific model for estimating the weighted mean temperature of the atmosphere. J Geod 86:1125–1135

Yao YB, Zhang B, Yue SQ, Xu CQ, Peng WF (2013) Global empirical model for mapping zenith delays onto precipitable. J Geod 87:439–448

Yao YB, Zhang B, Xu CQ, Chen JJ (2014a) Analysis of the global $T_m − T_s$ correlation and establishment of the latitude-related linear model. Chin Sci Bull 59(19):2340–2347

Yao YB, Zhang B, Xu CQ, Yan F (2014b) Improved one/multiparameter models that consider seasonal and geographic variations for estimating weighted mean temperature in ground-based GPS meteorology. J Geod 88(3):273–282

Yao YB, Xu CQ, Zhang B, Cao N (2014c) GTm-III: a new global empirical model for mapping zenith wet delays onto precipitable water vapor. Geophys J Int 197:202–212

Yao CL, Luo ZC, Liu LL, Zhou BY (2015a) On the relation between the wet delay and the water precipitable vapor in consideration of topographic relief in the low-latitude region of China. Geomat Inform Sci Wuhan Univ 40(7):907–912

Yao YB, Xu CQ, Zhang B, Cao N (2015b) A global empirical model for mapping zenith wet delays onto precipitable water vapor using GGOS Atmosphere data. Sci China Earth Sci 58:1361–1369

Yao YB, Xu CQ, Shi JB, Cao N, Zhang B, Yang JJ (2015c) A new global GNSS tropospheric correction model. Sci Rep 5:10273

Zhang HX, Yuan YB, Li W, Ou JK, Li Y, Zhang BC (2017) GPS PPP-derived precipitable water vapor retrieval based on Tm/Ps from multiple sources of meteorological data sets in China. J Geophys Res Atmos. https://doi.org/10.1002/2016JD026000

Zhao QZ, Yao YB, Yao WQ (2018) GPS-based PWV for precipitation forecasting and its application to a typhoon event. J Atmos Sol Terr Phys 167:124–133